InP-Based Optical Waveguide MEMS Switches With Evanescent Coupling Mechanism

Marcel W. Pruessner, *Student Member, IEEE*, Kuldeep Amarnath, Madhumita Datta*, Member, IEEE*, Daniel P. Kelly, S. Kanakaraju, Ping-Tong Ho, and Reza Ghodssi*, Member, IEEE*

***Abstract*—An optical waveguide MEMS switch fabricated on an indium phosphide (InP) substrate for operation at 1550 nm wavelength is presented. Compared to other MEMS optical switches, which typically use relatively large mirrors or long end-coupled waveguides, our device uses a parallel switching mechanism. The device utilizes evanescent coupling between two closely-spaced waveguides fabricated side by side. Coupling is controlled by changing the gap and the coupling length between the two waveguides via electrostatic pull-in. This enables both optical switching and variable optical coupling at voltages below 10 V. Channel isolation as high as −47 dB and coupling efficiencies of up to 66% were obtained with switching losses of less than 0.5 dB. We also demonstrate voltage-controlled variable optical coupling over a 17.4 dB dynamic range. The devices are compact with 2 μm × 2 μm core cross section and active area as small as 500 μm × 5 μm. Due to the small travel range of the waveguides, fast operation is obtained with switching times as short as 4 μs. Future devices can be scaled down to less than 1 μm × 1 μm waveguide cross-sectional area and device length less than 100 μm without significant change in device design. [1372]**

***Index Terms*—Directional coupler, indium phosphide (InP), integrated waveguides, optical MEMS switches.**

I. Introduction

ALL-OPTICAL networks promise large bandwidth and information carrying capacity [1]. These networks consist of optical fibers for transporting information over long distances. Optical switches are used for manipulating the optical signals directly rather than converting them into the electrical domain for manipulation, thereby reducing power consumption and increasing network speed and data integrity. All-optical data manipulation is enabled by optical integrated circuits (OICs), or integrated optics [2].

Manuscript received July 3, 2004; revised March 6, 2005. This work was supported by a National Science Foundation (NSF) CAREER award (R. Ghodssi) and by the Laboratory for Physical Sciences (LPS). Subject Editor O. Solgaard.

M. W. Pruessner, M. Datta, D. P. Kelly, and R. Ghodssi are with the MEMS Sensors and Actuators Lab, The Institute for Systems Research, University of Maryland, College Park, MD 20742 USA. They are also with the Department of Electrical and Computer Engineering, University of Maryland, College, Park, MD 20742 USA and the Laboratory for Physical Sciences, College Park, MD 20740 USA (e-mail: marcelp@glue.umd.edu; mdatta@glue.umd.edu; dpkelly@glue.umd.edu; ghodssi@eng.umd.edu).

K. Amarnath and P.-T. Ho are with the Department of Electrical and Computer Engineering, University of Maryland, College, Park, MD 20742 USA. They are also with the Laboratory for Physical Sciences, College Park, MD 20740 USA (e-mail: akuldeep@glue.umd.edu; ho@eng.umd.edu).

S. Kanakaraju is with the Department of Electrical and Computer Engineering, University of Maryland, College, Park, MD 20742 USA (e-mail: sk@lps.umd.edu).

Digital Object Identifier 10.1109/JMEMS.2005.851848

MEMS have unique advantages for optical communication applications [3], [4]. For one, the required displacements in optical switches and tunable filters are around one wavelength ($\sim 1\ \mu$m) or less and are well suited to MEMS actuators. Also, batch fabrication enables great cost savings compared to macro-scale devices and enables a large number of input/output ports on a single chip with low-loss.

Indium phosphide (InP) is attractive for optical communications due to its suitability as a substrate material for active optical devices made of indium gallium arsenide phosphide (InGaAsP) [5] operating at the $\lambda = 1550$ nm wavelength. Therefore, optical switches fabricated in InP can monolithically integrate lasers or semiconductor optical amplifiers (SOAs). In this manner, losses can be compensated on-chip without the need for separate optical amplifiers—a significant cost savings. Although InP-based MEMS have been previously demonstrated, most efforts have concentrated on vertical cavity tunable optical filters [6]–[12]. The tuning range for these optical filters is around 100 nm with similar actuation displacements. While InP is brittle, it has previously been shown to be sufficiently robust for MEMS applications [13]. Furthermore, we have already demonstrated InP-based electrostatic actuators with 1.8 μm displacement [14]. Such displacements enable all-optical switching.

Compared to free-space optical MEMS switches, which use large mirrors, moving waveguide MEMS switches are compact and enable large-scale integration while limiting losses due to the tight optical confinement within the waveguides. This is especially true for InP, which has a large refractive index ($n = 3.17$) at $\lambda = 1550$ nm wavelength [15]. Previously reported devices utilize a coupling mechanism in which an input waveguide is actuated to end couple with one of several output waveguides. Such devices have been realized in silica/SiO_2 on silicon [16], [17], GaAs/AlGaAs [18], and polymers on silicon-on-insulator [19] with operating voltages as low as 3.3 V [18], switching times as low as 32 μs [18], losses of 0.5 dB (0.05 dB with index-matching oil) and less than −52 dB crosstalk [17].

Our coupling mechanism differs from previous approaches. The device comprises two closely-spaced parallel waveguides. Coupling is controlled by changing the waveguide gap. The coupling mechanism relies on the evanescent optical field just outside of the waveguide—a field that decays exponentially with distance. Consequently, we require only very small displacements ($< 1\ \mu$m) for optical switching, resulting in very compact devices. Our approach also enables low-loss variable optical coupling, which is useful to tap a small fraction of power to measure the signal integrity of a network.

1057-7157/$20.00 © 2005 IEEE

We will use the following nomenclature and device designations in this paper (W = waveguide width, gap = waveguide separation):

L device length; length of movable waveguide segment;

L_{PI} measured waveguide pull-in length and physical coupling length;

L_C theoretical characteristic coupling length (results in 100% coupling);

Coupler 1a $L = 500\ \mu m$, $W = 2\ \mu m$, $gap = 1\ \mu m$ (pull-in actuation);

Coupler 2a $L = 1000\ \mu m$, $W = 2\ \mu m$, $gap = 2\ \mu m$ (pull-in actuation);

Coupler 2b $L = 1000\ \mu m$, $W = 2\ \mu m$, $gap \leq 2\ \mu m$ (pull-in actuation; stiction);

Coupler 3b $L = 3000\ \mu m$, $W = 2\ \mu m$, $gap \leq 2\ \mu m$ (pull-in actuation; stiction);

Coupler C-D $L = 4000\ \mu m$, $W = 2\ \mu m$ (comb-drive actuation).

II. Evanescent Coupling

A. Theory

Evanescent couplers are commonly used in optical communications as passive power splitters [20]. In optical fibers and waveguides part of the optical power travels outside of the core. This field, called the evanescent field, decays exponentially away from the fiber/waveguide. If two identical single-mode fibers or waveguides are brought close together, then the compound structure supports two optical modes: even and odd. These even and odd modes travel with different propagation constants and interfere constructively or destructively along different points z in the waveguide [21] (Fig. 1). This varying degree of interference enables optical switches to be realized.

Coupling between two identical waveguides is described by the coupled-mode equations [22]:

$$\frac{dA_{\mathrm{BAR}}(z)}{dz} = -i\beta A_{\mathrm{BAR}}(z) - i\kappa A_{\mathrm{CROSS}}(z) \text{ and} \quad (1a)$$

$$\frac{dA_{\mathrm{CROSS}}(z)}{dz} = -i\beta A_{\mathrm{CROSS}}(z) - i\kappa A_{\mathrm{BAR}}(z) \quad (1b)$$

where A_{BAR} and A_{CROSS} are the electric field amplitude in the BAR and CROSS waveguides (see Fig. 1), respectively, β is the propagation constant for each isolated waveguide, and κ is the coupling coefficient. The solution of the coupled-mode equations determines the amount of optical coupling. If the separation (gap) between the two fibers or waveguides and the physical coupling length ($z = L_{\mathrm{PI}}$) between them are chosen carefully, any fraction of power can be coupled from the BAR to the CROSS waveguide [21], [22]

$$P_{\mathrm{BAR}} = P_{\mathrm{IN}} \cos^2(\kappa \cdot L_{\mathrm{PI}}), \quad (2a)$$

$$P_{\mathrm{CROSS}} = P_{\mathrm{IN}} \sin^2(\kappa \cdot L_{\mathrm{PI}}), \quad (2b)$$

$$\kappa \sim \exp(-\mathrm{gap}) \quad (3)$$

where we have assumed $P_{\mathrm{BAR}}(z = 0) = P_{\mathrm{IN}}$, $P_{\mathrm{CROSS}}(z = 0) = 0$ and negligible waveguide losses. The reader should be aware that we refer to L_{PI} instead of the device length, L, in the equations above since the coupling length is determined by the *pull-in length*.

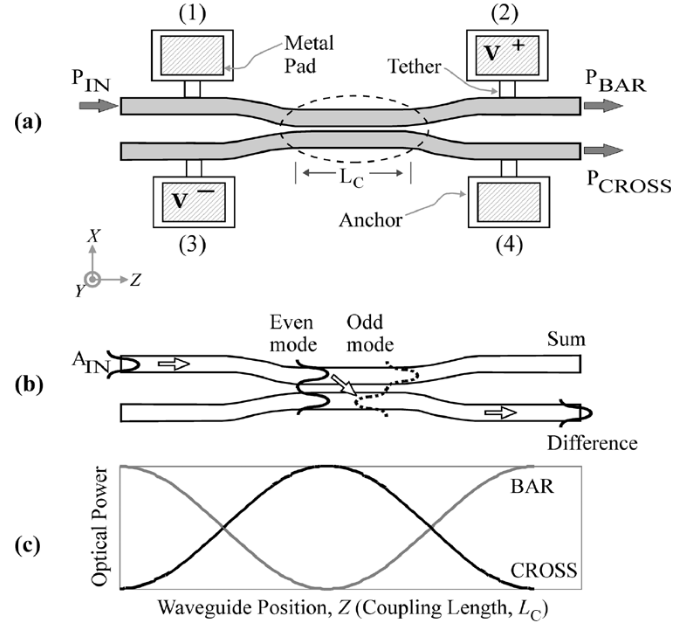

Fig. 1. (a) Top view schematic (in actuated state with waveguides pulled-in), (b) optical coupling via interference of odd and even modes, and (c) variation of coupled optical power in the BAR and CROSS outputs as a function of position along the length of the waveguide. Note that (b) represents the electric fields; the optical power in (c) is $P = |A|^2$.

The MEMS coupler takes advantage of the exponential decay of the evanescent field. By varying the spacing between two parallel, *movable* waveguides, we can perform a switching operation. The top-view device schematic is shown in Fig. 1(a). For 1–2 μm gaps, we expect no optical coupling due to the exponential decay of the evanescent field. However, at pull-in the gap is around 100 nm (depending on the sidewall roughness and verticality) and coupling will proceed as in Fig. 1(b) and (c).

B. Advantages of MEMS-Based Couplers

Passive evanescent couplers are commonly used as optical splitters. Active couplers have used integrated thin-film heaters to perform optical switching by varying the refractive index, n, between two *fixed* parallel waveguides [23]. However, these devices typically consume significant power (tens of mW). Other approaches have utilized expensive electrooptic materials [24] to vary n and achieve switching by application of an electric field.

The device presented here uses electrostatic "pull-in" actuation to vary the spacing between two *movable* suspended waveguides. The actuation distances are 1–2 μm, resulting in low-power and high-speed operation (compared to electrothermal couplers [23]). This also results in a large ON/OFF contrast and low crosstalk due to the exponential dependence of optical coupling on the waveguide gap. A similar approach has been proposed in the past [25], [26] with large attenuation (−65 dB) at low actuation voltages (2.5 V) obtained experimentally, although successful switching was not demonstrated. Optical switches using MEMS-actuated evanescent coupling in gallium arsenide waveguides were simulated in [27], and

MEMS-actuated displays using cantilevers and evanescent coupling were experimentally demonstrated in [28]. Successful coupling between a movable silicon waveguide and a fixed micro-disk resonator optical filter was also recently demonstrated [29]. However, the moving waveguide segment was short (100 μm length), resulting in a large actuation voltage (120 V). Optical wavelength-selective switching was demonstrated using a ring-resonator filter and an electrostatically-actuated membrane [30]. This device behaved as an optical filter ($V = 0$), but became wavelength-insensitive (all-pass) when the membrane was pulled-in to the ring-resonator (~20 V).

Our device utilizes moderately doped semiconductor waveguides with small gaps (1–2 μm) in order to ensure low-voltage operation. The fabrication process is simple compared to [25], [26] since our waveguides are parallel and actuated in-plane rather than out-of-plane, resulting in a self-aligned process without the need for wafer bonding. Compared to [29], [30], couplers are relatively wavelength insensitive. Finally, InP enables integration of active devices with optical gain at 1550 nm. However, for passive operation our device can also be fabricated in inexpensive materials—i.e., polymer or SiO_2/SiN waveguides on silicon actuators, or even silicon/SOI waveguides—without significant design changes.

III. Device Design and Fabrication

A. Layer Structure

The InP MEMS structure (see Fig. 2) is grown by molecular beam epitaxy (MBE). We designed a waveguide core with $In_{0.96}Ga_{0.04}As_{0.08}P_{0.92}$ and a cladding with $In_{0.99}Ga_{0.01}As_{0.01}P_{0.99}$. The small gallium (Ga) and arsenic (As) mole fractions do not change the mechanical properties of InP significantly, but they enable fine tuning of the refractive index, bandgap, and intrinsic strain. These layers were chosen to obtain refractive indices $n_{\mathrm{CORE}} = 3.195$ and $n_{\mathrm{CLADDING}} = 3.173$ using data from [31].

The layer structure was designed with a bandgap waveglength $\lambda_g = 950$ nm, much less than the operating wavelength $\lambda = 1550$ nm so that it is a truly passive waveguide. During electrostatic actuation the electric field is confined to the air gap region between the waveguides, not within the waveguides themselves, so any electro-optic effect is minimal [32], [33]. Furthermore, the variation of waveguide spacing produces a change in coupling that is orders of magnitude greater than any change in coupling due to modulation of the refractive index resulting from an applied electric field.

Mechanically, the waveguide was designed to be under slight tensile strain ($\varepsilon < 0.05\%$) so that doubly-clamped structures remain flat and aligned vertically [14]. The gallium (Ga) and arsenic (As) mole fractions also control the intrinsic strain. For sacrificial wet etching we require complete selectivity between the waveguides and the sacrificial layer. We chose InP waveguides and a lattice-matched $In_{0.53}Ga_{0.47}As$ sacrificial layer, which results in complete selectivity when etching in $HF : H_2O_2 : H_2O$.

For electrostatic actuation, the waveguides are moderately doped. We limit the doping level to $n = 5 \times 10^{17}/\mathrm{cm}^3$ in order

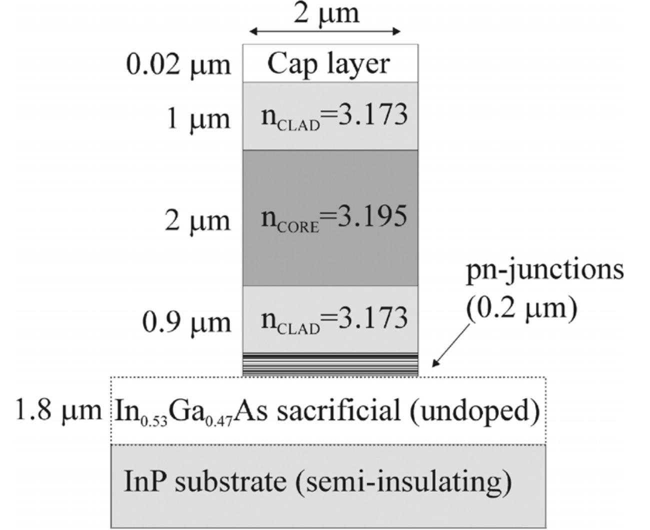

Fig. 2. Layer structure and waveguide geometry. The waveguides are doped $n = 5 \times 10^{17}/\mathrm{cm}^3$ and are designed to be under slight tensile strain ($\varepsilon < 0.05\%$). The core and cladding refractive indices are $n_{\mathrm{CORE}} = 3.195$ (for $In_{0.96}Ga_{0.04}As_{0.08}P_{0.92}$) and $n_{\mathrm{CLADDING}} = 3.173$ ($In_{0.99}Ga_{0.01}As_{0.01}P_{0.99}$) at 1550 nm wavelength. The cap layer is InP with $n \sim 10^{19}/\mathrm{cm}^3$.

to reduce optical losses due to free carrier absorption; n-type doping was chosen since p-type gives larger absorption [34].

B. Optical Design

The MEMS evanescent coupler utilizes our suspended waveguide technology [35]. Here, the waveguides are suspended in air above the substrate by 1.5 μm wide tethers spaced 1000–2000 μm apart. Optical coupling in our device depends on the waveguide separation, the physical coupling length, L_{PI}, and the optical polarization. We obtain the coupling coefficient, κ, by simulating [36] the effective refractive index for even and odd modes (n_{even} and n_{odd}) for the 2 μm wide waveguides and subsequently calculating the coupling coefficient, κ, and L_{C} [21], [22]:

$$\kappa = \frac{(\beta_{\mathrm{even}} - \beta_{\mathrm{odd}})}{2} = \frac{(n_{\mathrm{even}} - n_{\mathrm{odd}})k_o}{2} \quad (4)$$

$$L_{\mathrm{C}} = \frac{\pi}{2\kappa} \quad (5)$$

where $k_o = 2\pi/\lambda_o$ and $\lambda_o = 1550$ nm is the free-space wavelength. Here, L_C is the characteristic length that results in 100% coupling from the BAR to the CROSS waveguide; so, ideally, we want $L_{\mathrm{C}} = L_{\mathrm{PI}}$.

The simulated characteristic coupling length, L_{C}, versus waveguide separation is shown in Fig. 3(a), along with the corresponding coupling coefficient, κ. Looking at the simulation result, we note that S-polarization (TE-modes, electric field perpendicular to wafer plane) results in significantly shorter L_C than P-polarization (TM-modes, electric field parallel to wafer plane) for our waveguides. We expect eight times as efficient coupling for S-polarization compared to P-polarization [see Fig. 3(b)]. Compact devices with coupling lengths of only a few hundred microns are feasible. Also, changing the gap from 100 nm to 600 nm effectively turns the device from completely "ON" (100% coupling) to "OFF" (negligible coupling). This

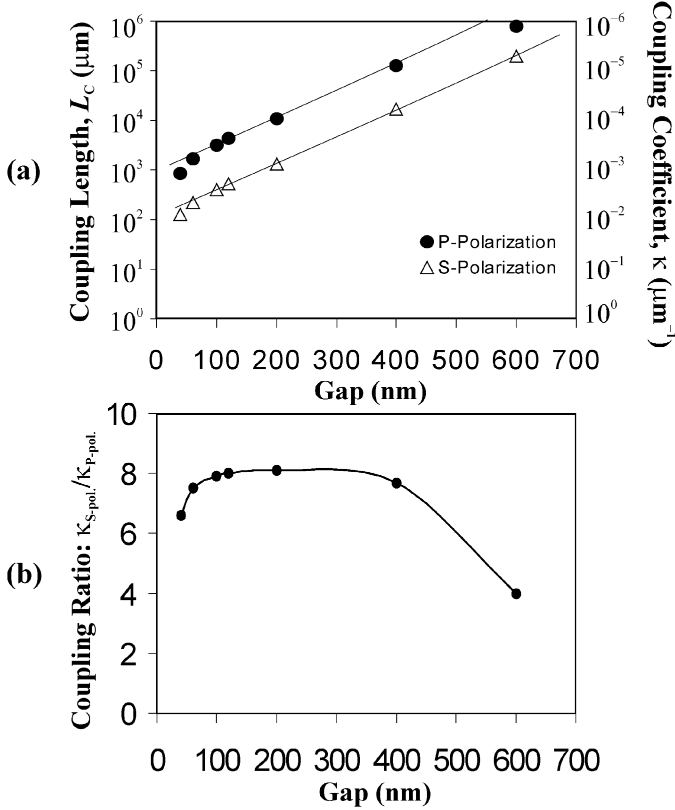

Fig. 3. (a) Simulated characteristic coupling length (L_C) for 100% transfer of power from BAR to CROSS waveguide as a function of waveguide separation (gap) for S- (TE) and P-polarizations (TM). The corresponding coupling coefficient (κ) is also shown. (b) Polarization-dependent coupling: S-polarization results in roughly eight times as efficient coupling compared to P-polarization.

enables high-speed and low-power switching due to the small actuation distance required.

C. Mechanical Design

For the mechanical design we calculate the pull-in voltage as a function of waveguide length, assuming 2 μm wide, 4 μm tall structures. Although our device consists of two movable parallel suspended waveguides, we model our device as a single doubly-clamped waveguide over an infinite plane placed at half the waveguide-to-waveguide gap. This half-structure model lets us use standard pull-in equations [37] to obtain an estimate of the switching voltages of our device. The device pull-in voltage is twice the voltage obtained from the half-structure model. In Table I the pull-in voltage for various device geometries is shown. For all calculations the Young's modulus is $E = 90$ GPa [14] and the intrinsic tensile stress is $\sigma = 45$ MPa (by design).

D. Fabrication

Fabrication of the MEMS coupler is described in our previous work [38]. We deposit 7000 A SiO_2 on 15 mm × 15 mm chips. Next, we pattern positive photoresist via projection lithography followed by reactive ion etching (RIE) of the SiO_2 mask. Methane-hydrogen RIE is used to etch the InP waveguides to a depth of greater than 5 μm with verticality of better than 85 degrees. After stripping the SiO_2 mask in BHF,

TABLE I
CALCULATED PULL-IN VOLTAGE FOR VARIOUS COUPLER DESIGNS

L (μm)	*Gap* (μm)	V_{PI}(V)
500	1	7.11
1000	2	9.07
2000	2	4.38
3000	2	2.89
1000	3	16.29
2000	3	7.86
3000	3	5.18

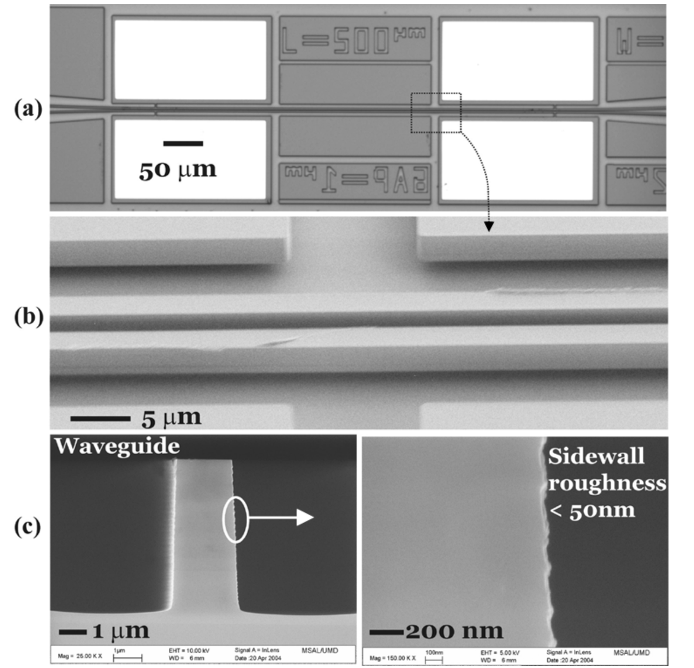

Fig. 4. (a) Top view of fabricated coupler switch, (b) SEM of suspended 2 μm wide waveguides, and (c) cleaved test waveguide before sacrificial etch with detail of sidewall roughness. This particular device (*coupler 1a*) has a 1 μm nominal gap before actuation [(a), (b)]. Other devices have a 2 μm nominal gap.

Ni-Au-Ge-Ni-Au ohmic contacts are patterned via electron beam evaporation and lift-off in acetone. An annealing step is then performed in an N_2/H_2 atmosphere (400° C, 40 sec.) to alloy the metal contacts. Next, we thin the samples to $\sim 200\ \mu$m thickness and cleave the input and output waveguides to obtain optical-quality facets for coupling light to our chip. Finally, we perform sacrificial etching of the $In_{0.53}Ga_{0.47}As$ layer with HF : H_2O_2 : H_20 (1:1:8) followed by supercritical CO_2 drying. A released coupler is shown in Fig. 4, indicating less than 50 nm sidewall roughness. This determines the approximate coupling gap during pull-in, which will be twice the sidewall roughness, or 100 nm.

IV. EXPERIMENTAL RESULTS

A. Experimental Setup

All devices were tested at 1550 nm wavelength with S-polarization (E-field out of the wafer plane, TE-modes), unless otherwise stated. The experimental setup consisted of a tunable laser set to 1550 nm, a polarization control unit and input/output lensed fibers controlled by electrostrictive XYZ-stages. A probe station and function generator were used

to actuate the device, and the electrical actuation signals and measured optical output power were fed to an oscilloscope. We used a microscope and charge-coupled device (CCD) camera to image the device during testing to ascertain that coupling was indeed resulting from the variation in waveguide separation.

B. Electrostatic Actuation

The present devices are electrostatically actuated—in contrast to our previously demonstrated devices, which were electro-thermally actuated [38]. Fig. 5 shows the measured pull-in voltage for various waveguide lengths and gaps along with calculations (material properties: $E = 90$ GPa, $\sigma = 45$ MPa intrinsic stress). Measurements were performed on dedicated pull-in test structures rather than on the couplers themselves. The results indicate good agreement with calculations using pull-in equations for doubly-clamped beams [37].

Short devices ($L = 500$ μm, *coupler 1a*) operated very reliably for actuation at the pull-in voltage. *Coupler 1a* proved reliable even at low-frequency ($f < 0.1$ Hz) operation as long as the actuation voltage did not exceed the initial pull-in voltage significantly. Longer and more compliant devices, however, ($L \geq 1000$ μm, *coupler 2b* and *coupler 3b*) suffer from stiction [39] after initial or repeated pull-in when low-frequency actuation ($f \leq 100$ Hz) is used. For high frequency operation ($f \geq 1$ kHz), reliable operation was obtained for $L = 1000$ μm devices (*coupler 2a*) with no observable stiction effects. In excess of 10 million switching cycles have been performed with *coupler 2a* at $f = 10$ kHz with no change in device performance. Therefore, although stiction may affect long-term device reliability, the experiments indicate that short devices with large spring constant can exhibit very reliable operation, provided that proper operating conditions (actuation voltage, frequency) are met. Later on, in Section V, we present some alternative designs to the pull-in couplers that do not rely on pull-in actuation.

Current flow during pull-in is also a concern. Landing electrodes or mechanical stops are a possible solution for preventing stiction and current flow. However, for efficient optical coupling very small waveguide gaps (~100 nm) are required, so that fabrication of precise mechanical landing structures becomes a challenge. Concerning pull-in current, the waveguides are doped $\mathrm{n} = 5\times10^{17}/\mathrm{cm}^3$ with typical resistance of $10\,\Omega/\mu\mathrm{m}$ unit length. We measured a current of 1.5 μA during pull-in for *coupler 2a*, which is sufficiently small to prevent heating. We also measured the pull-in current for *coupler 2b* after stiction occurs. While the current is increased slightly, it is limited to less than 25 μA for actuation voltages up to 7 V, so heating is minimal. Future devices can utilize waveguides with lower doping level to reduce pull-in current flow. Alternatively, $\mathrm{SiO_2}$ or SiN_X can be deposited on the waveguide sidewalls. This will prevent any current flow and will also reduce stiction effects.

C. Tether, Waveguide Propagation, and Insertion Losses

In our MEMS couplers, the waveguides are suspended above the substrate via tethers [35]. The waveguide propagation loss was previously measured to be 2.2 dB/cm [35], which includes

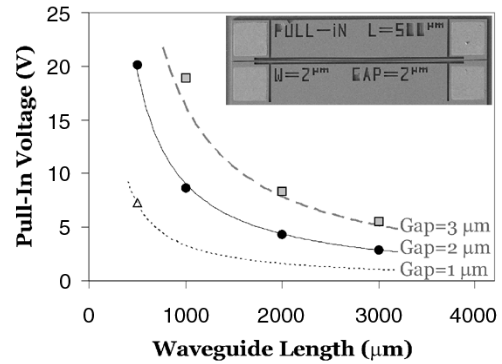

Fig. 5. Simulated (lines) and measured (symbols) pull-in voltage for various coupler test structures. Inset: test structure for measuring pull-in voltage.

scattering losses due to sidewall roughness as well as material losses. Each tether pair introduces an additional 0.25 dB of loss. These loss figures are comparable to other III-V semiconductor waveguides [40]. Rib (ridge) waveguides generally have a larger cross-sectional area, which reduces scattering losses since the mode propagates far from the waveguide surface and does not experience significant sidewall roughness.

The fiber-to-chip coupling loss dominates the insertion loss. It is about 10 dB at the input and output of the coupler, resulting in 20 dB total loss. Such losses are to be expected given the inherent differences in the mode-shape of the lensed fibers compared to the mode-shape of the InP waveguides. By utilizing tapers at the input and output waveguides, coupling losses can be significantly reduced [41].

D. Optical Switching

Various couplers of different lengths and gaps were tested. *Coupler 1a* exhibited better than −47 dB crosstalk in the 'OFF' state [38]. We actuated the device at 8 Vp-p square wave ($f = 10$ Hz) and measured the $CROSS$ coupled power during actuation, which was $P_{\mathrm{CROSS}} = 10\%$. The reason for the small coupling is the short coupling length obtained as well as the waveguide separation at pull-in. We measured a coupling length of $L_{\mathrm{PI}} = 225$ μm (Fig. 6). Using (2), we obtain $\kappa_{\mathrm{S-pol}} \cdot L_{\mathrm{PI}} = 0.322$, resulting in a coupling coefficient $\kappa_{\mathrm{S-pol}} = 1.43 \times 10^{-3}/\mu\mathrm{m}$. From the simulation (Fig. 3) we see that this coupling coefficient indicates a waveguide gap of 200 nm at pull-in, a reasonable value considering sidewall roughness and sidewall angle. For longer devices we expect similar $\kappa_{\mathrm{S-pol}}$, but increased coupling length, L_{PI}, and hence increased coupled power P_{CROSS}.

A longer device (*coupler 2b*) is shown in Fig. 7. Although stiction is present in this device after initial pull-in, the stiction region is small (solid circle) and for most of the device the waveguides are sufficiently far apart to prevent significant optical coupling. Furthermore, because the waveguides are not completely vertical, the actual contact area is very small—close to the bottom the waveguides are in contact and closer to the top the measured gap is 750 nm in the 'OFF' state. This results in a large contact resistance between the waveguides with measured R_{stiction} greater than 1 MΩ. This is significantly larger than the

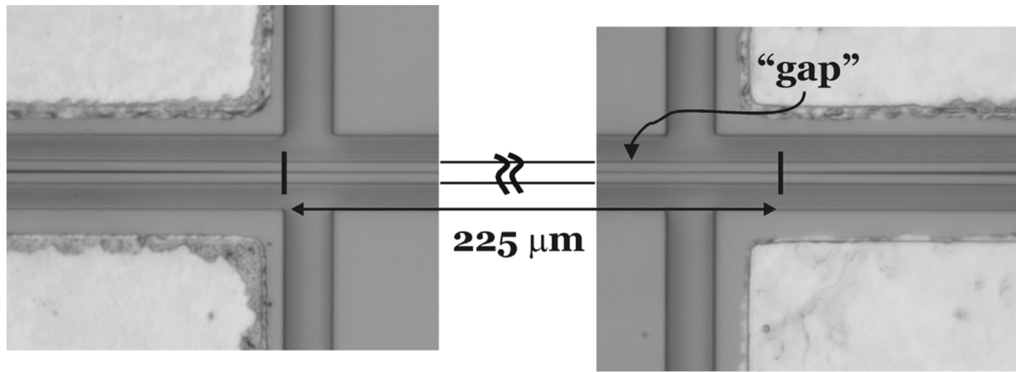

Fig. 6. Measured coupling length for electrostatically actuated *coupler 1a* during pull-in. The measured coupling length is $L_{\rm PI} = 225\ \mu{\rm m}$. Note that the device has a small but visible gap separating the waveguides during pull-in.

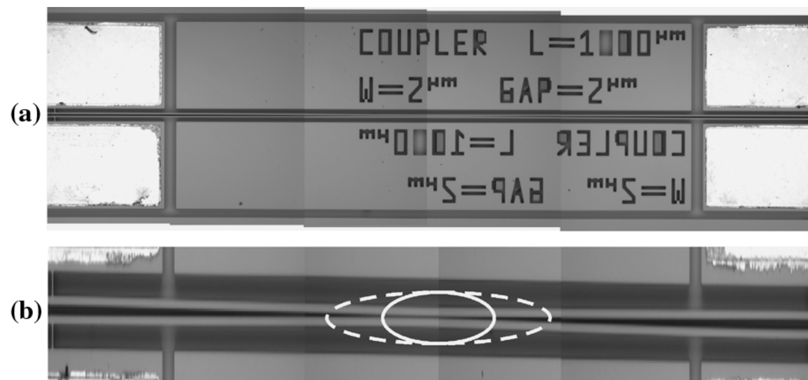

Fig. 7. (a) *Coupler 2b* after actuation and subsequent stiction, (b) detail of center region (note: image height has been stretched in order to show detail of stiction region). With $V = 0$ the coupled region is small (solid circle) and with $V > 0$ the coupling region increases (dashed circle).

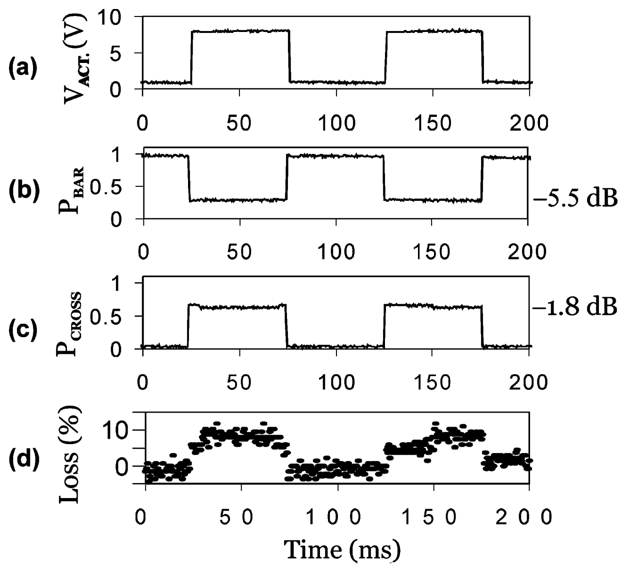

Fig. 8. Optical response for *coupler 2b*: (a) actuation signal, (b) measured optical BAR output, (c) measured optical $CROSS$ output, and (d) coupling loss, defined as $loss = 1 - (P_{\rm BAR} + P_{\rm CROSS})$. Both $P_{\rm BAR}$ and $P_{\rm CROSS}$ are normalized to $P_{\rm MAX}$.

waveguide resistance, which is $10\ \Omega/\mu{\rm m}$ (i.e., a $1000\ \mu{\rm m}$ waveguide has $R = 10\ k\Omega$). Therefore, we can still electrostatically actuate the waveguides in the stiction state.

The optical response of the device is shown in Fig. 8. In the "OFF" state, we measure 1.2% $CROSS$ coupled power ($V = 0$). This results in −19.2 dB channel isolation. At $V = 8$ Vp−p we obtain 66% CROSS coupled power and a minimum uncoupled BAR power during actuation of 25%. The switching loss, defined as $loss = 1 - (P_{\rm BAR} + P_{\rm CROSS})$, is less than 10% (0.45 dB). For actuation at 8 Vp-p the measured coupling length is $L_{\rm PI} = 550\ \mu{\rm m}$, from which we obtain the coupling coefficient $\kappa_{\rm S-pol} = 1.72 \times 10^{-3}/\mu{\rm m}$. Comparing the two couplers, we find that the coupling coefficient for *coupler 2b* is similar to *coupler 1a* ($\kappa_{\rm S-pol} = 1.43 \times 10^{-3}/\mu{\rm m}$). Looking at the simulations, we expect a 190 nm coupling gap during pull-in for *coupler 2b*, similar to the 200 nm gap obtained for *coupler 1a*.

E. Switching Speed

The measured switching speed of three electrostatically actuated couplers (*coupler 1a*, *coupler 2a*, and *coupler 2b*) is shown in Fig. 9. The risetime [Fig. 9(a), (c), and (e)] exhibits a delay before optical coupling occurs due to the waveguide travel time, the time required for the waveguides to come into sufficiently close contact in order for optical coupling to occur. It is interesting to note that *coupler 1a* and *coupler 2a* exhibit a clear delay (10 μs, 18 μs) due to the 1–2 $\mu{\rm m}$ gap [see Fig. 9(a) and (c)]. *Coupler 2b* has a fairly small delay ($< 1\ \mu$s) resulting from the close proximity of the waveguides due to stiction [Fig. 9(e)]. This is in good agreement with theory: due to the exponential dependence of the coupling coefficient on the waveguide separation, only small gaps (∼100 nm) result in measurable optical coupling. For this same reason, the falltime [see Fig. 9(b), (d),

TABLE II

SUMMARY OF MEASURED P_{CROSS} AND PHYSICAL COUPLING LENGTH, L_{PI}, FOR DIFFERENT DEVICES AND ACTUATION VOLTAGES. THE EXTRACTED COUPLING COEFFICIENT, $\kappa_{\mathrm{S-pol.}}$, AND THE CHARACTERISTIC COUPLING LENGTH, L_{C}, FOR S-POLARIZATION ARE ALSO GIVEN

Device (Actuation Voltage)	Measured Coupled Power, P_{CROSS} (norm.)	Measured Coupling Length, L_{PI} (μm)	Extracted Coupling Coefficient, $\kappa_{S\text{-}pol.}$ (μm^{-1})	Extracted Characteristic Coupling Length, $L_C=\pi/2\kappa_{S\text{-}pol.}$ (μm)
Coupler 1a (V = 7.5 Vp-p)	0.10	225	1.43×10^{-3}	1098
Coupler 2b (V = 6 Vp-p)	0.30	390	1.51×10^{-3}	1040
Coupler 2b (V = 8 Vp-p)	0.66	550	1.72×10^{-3}	913

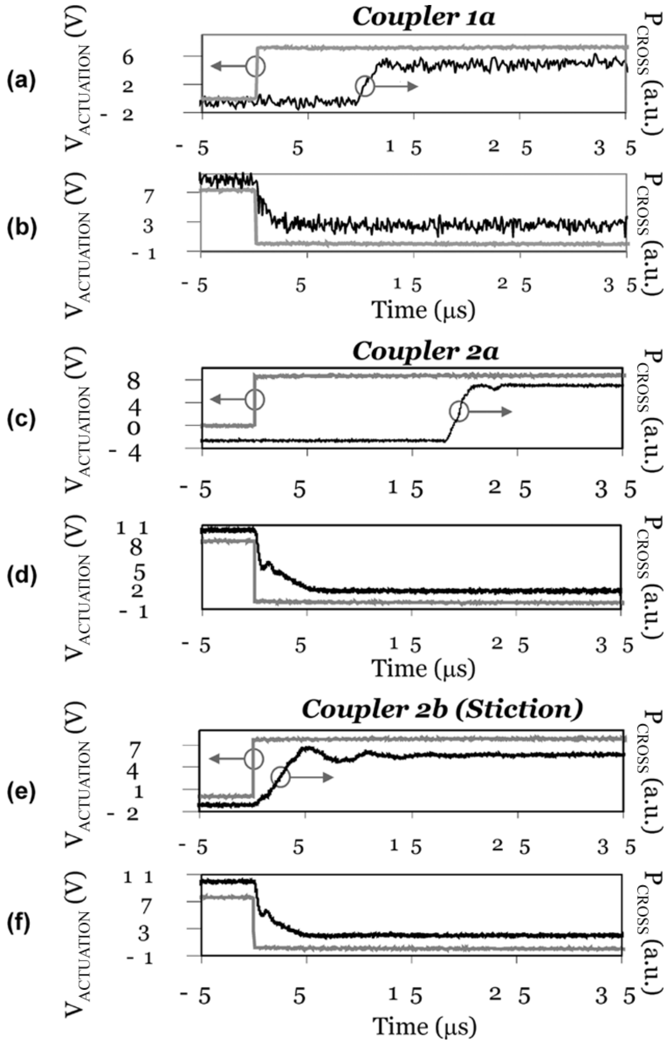

Fig. 9. Switching speed of several electrostatically actuated MEMS couplers: (a) risetime for *coupler 1a*, (b) falltime for *coupler 1a*, (c) risetime for *coupler 2a*, (d) falltime for *coupler 2a*, (e) risetime for *coupler 2b* $(gap \ll 2\ \mu\mathrm{m})$, and (f) falltime for *coupler 2b* $(gap \ll 2\ \mu\mathrm{m})$.

and (f)] does not show a delay since the beams separate immediately upon removal of the actuation signal and optical coupling decreases. The fastest switching speed we obtained was 4 μs (*coupler 2b*). Concerning switching frequency, we actuated our devices up to 25 kHz (*coupler 1a*) with no change in device performance.

F. Variable Optical Coupling

The devices discussed above are switches and are digital in nature: they are either "ON" or "OFF." However, the amount of optical coupling can be controlled by varying either the waveguide gap or the coupling length. Due to the pull-in nature of our devices, we cannot continuously vary the waveguide gap to tune the amount of coupling. We now present experiments that involve varying the coupling length, L_{PI}, in order to achieve variable optical coupling.

Coupler 2b was shown in Fig. 7. The solid circle represents the coupling region in the rest state $(V = 0)$. As we increase the actuation voltage, the coupling length increases as the two waveguides come into contact over a larger length (dashed circle), resulting in increased optical coupling. The measured optical coupling as a function of actuation voltage is shown in Fig. 10(a). As the actuation voltage increases, coupling increases from -19.2 dB $(V = 0)$ until the device acts as a -3 dB splitter (7 Vp-p). Further increase in actuation voltage to 8 Vp-p results in 66% coupling (-1.8 dB). This represents a 17.4 dB dynamic variable coupling range with less than 10% loss. Such low-loss variable optical coupling is not possible with end-coupled switches [16]–[19] in which any uncoupled power is lost. Therefore, our MEMS evanescent coupler has a unique advantage over other MEMS-based approaches.

The coupling lengths for this device (*coupler 2b*) were measured at 6 Vp-p and 8 Vp-p actuation, resulting in $L_{\mathrm{PI}} = 390\ \mu\mathrm{m}$ and $550\ \mu\mathrm{m}$, respectively. As before, we calculate the coupling coefficients and obtain $\kappa_{\mathrm{S-pol}} = 1.51 \times 10^{-3}/\mu\mathrm{m}$ and $\kappa_{\mathrm{S-pol}} = 1.72 \times 10^{-3}/\mu\mathrm{m}$, respectively. The results are summarized in Table II and are in general agreement with the coupling coefficient obtained for *coupler 1a*, which had $\kappa_{\mathrm{S-pol}} = 1.43 \times 10^{-3}/\mu\mathrm{m}$. In our experiments the measured coupling coefficient increases slightly with both increasing device length as well as increasing actuation voltage. This is likely due to the slight decrease in waveguide gap with increased actuation voltage. In addition, longer devices are more compliant and will also result in a slightly decreased actuation gap and increased coupling.

A second device (*coupler 3b*) initially behaves as a -3 dB power splitter due to stiction at $V = 0$ [see Fig. 10(b)]. The reason is that the stiction length, and hence the coupling length (L_{PI}), is longer than for *coupler 2b*. As the actuation voltage is increased, we increase L_{PI}, resulting in an initial decrease in the CROSS power and an increase in the BAR power [see

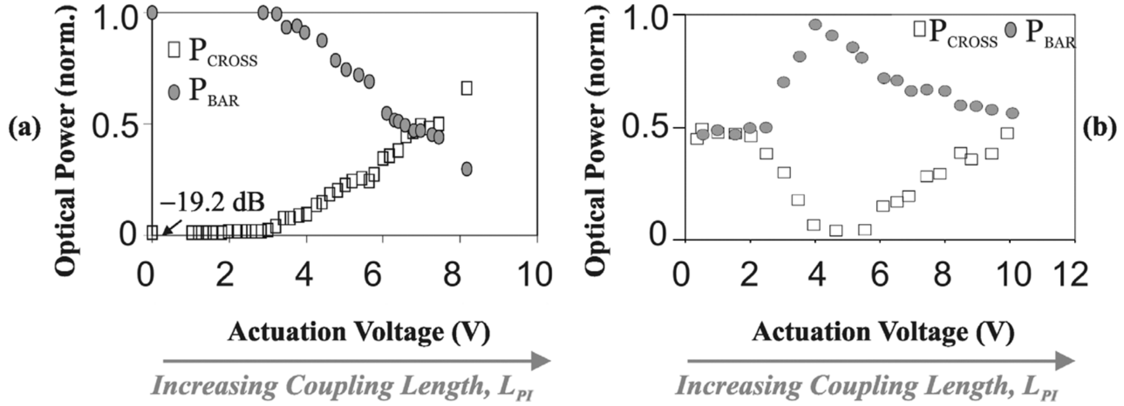

Fig. 10. (a) Variable coupling for *coupler 2b* and (b) variable coupling for *coupler 3b*. For *coupler 2b* an actuation voltage of $V = 6$ Vp − p causes an increase in $P_{\rm CROSS}$ while for *coupler 3b* an actuation voltage of $V = 5$ Vp − p causes a decrease in $P_{\rm CROSS}$.

Fig. 10(b)]. At $V = 5$ V we turn the device completely "OFF" so that all the optical power is in the BAR waveguide. By increasing the actuation voltage to 10 V we increase the CROSS power and decrease the BAR power arriving again at a −3 dB coupler. This clearly demonstrates the mode interference picture predicted by (1), (2) and Fig. 1(c).

While the above experiments utilized couplers and stiction, we note that similar experiments can be made with couplers that do not rely on pull-in actuation. From Table II we see that increased coupling length, $L_{\rm PI}$, results in larger coupled power. Alternatively, (2) tells us that an increased coupling coefficient, κ, can give us increased coupled power, since $P_{\rm CROSS} = \cos^2(\kappa L_{\rm PI})$. Smaller waveguide gaps result in larger coupling coefficient, κ. Therefore, variable optical coupling can also be achieved using actuators that enable continuous variation of the waveguide gap, such as comb-drives. To this end, a MEMS variable coupler with comb-drive actuation is presented in Section V.

G. Polarization and Wavelength Dependence

Polarization-dependent coupling was measured using *coupler 2b* (see Fig. 7) during actuation. The measured CROSS coupled power for both S-and P-polarizations during actuation is shown in Fig. 11. The results indicate 66% coupling for S-and 2.8% coupling for P-polarization. From the S-polarization measurement we obtain $\kappa_{\rm S-pol} \cdot L_{\rm PI} = 0.89$. Similarly, we obtain $\kappa_{\rm P-pol} \cdot L_{\rm PI} = 0.17$ for P-polarization. The polarization-dependent *coupling ratio* is then $\kappa_{\rm S-pol}/\kappa_{\rm P-pol} = 5.6$, which is in general agreement with the simulated value $\kappa_{\rm S-pol}/\kappa_{\rm P-pol} = 8$ [see Fig. 3(b)].

Some of the discrepancy between simulation and experiment is due to measurement error, taking into account scattered light in our measurement setup. We note that the coupled power for P-polarization is small (2.8%, or sub-μW levels) so that measurement errors are increased compared to S-polarization. Furthermore, some polarization conversion is to be expected in the waveguides due to sidewall roughness [42] and the trapezoidal waveguide cross-section. Therefore, if we input 100% P-polarized light into the *BAR* input, then some portion will be converted to S-polarized light resulting in increased coupling compared to 100% P-polarized light. A third factor is that the waveguides are not strictly single-mode so that higher order

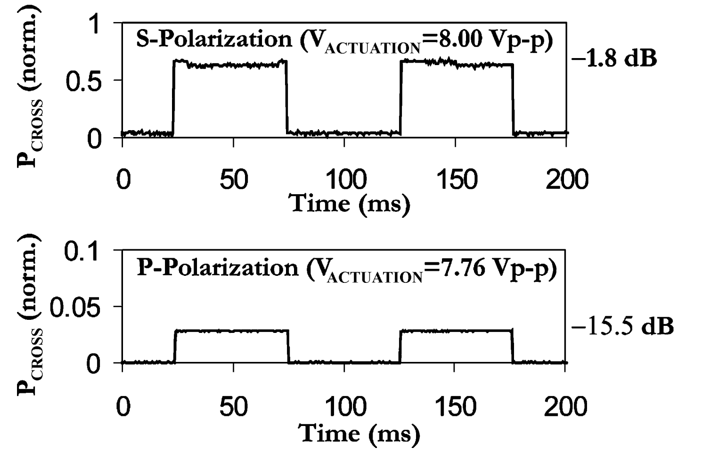

Fig. 11. Polarization-dependent coupling from BAR to CROSS waveguide for *coupler 2b*: S-polarization with 66% coupling (TE-modes, top), and P-polarization with 2.8% coupling (TM-modes, bottom).

modes may also contribute to the coupling. The simulations, in contrast, assume single-mode waveguides and therefore predict slightly lower coupling than we obtain experimentally. Nonetheless, the general agreement in predicting stronger coupling for S- compared to P-polarized light indicates that the simulations give a reasonable approximation for future device design.

Optical couplers also exhibit a slight wavelength-dependence. From (4) we see that the coupling coefficient, κ, is proportional to the wavevector $k_0 = 2\pi/\lambda$. Although $n_{\rm even}$ and $n_{\rm odd}$ in (4) are also wavelength-dependent, to first order the coupling coefficient has a simple relation to wavelength: $\kappa \sim k_0 \sim 1/\lambda$. Therefore, for small wavelength ranges centered about $\lambda_0 = 1550$ nm (typical WDM communications subbands span 20–30 nm range), the coupling coefficient is relatively wavelength insensitive.

While evanescent coupling results in polarization and some wavelength sensitivity, there are methods to overcome such dependence. For example, it has been shown that polarization-independent and wavelength-insensitive fixed couplers can be demonstrated by connecting two passive couplers in series with an optical phase shift [43], [44]. Such devices can be readily adapted to our device by cascading two MEMS couplers in series and actuating both of them simultaneously during switching. A second approach requires redesign of the

waveguide geometry. Polarization-insensitive MEMS couplers have been simulated by *Povinelli et al.* [27]. However, these devices required waveguides of $a = 280$ nm width and precise waveguide gaps of similar dimension a, which requires electron-beam lighography and is beyond the scope of this work.

V. Discussion

A. Remarks

Coupled-mode theory [21], [22] is accurate for waveguides that are weakly coupled. We chose our waveguide dimensions ($2\mu\text{m} \times 2\ \mu\text{m}$ core cross section) for mechanical robustness based on our prior work on similar dimensioned structures [14]. However, this results in a waveguide that supports more than one optical mode. Furthermore, one might argue that during pull-in the waveguides are in contact and therefore strongly-coupled so that the coupled-mode theory no longer applies.

The experimental results indicate that our devices can be modeled by single-mode waveguides. Looking at the single-mode simulations (Fig. 3), we see that for 100–200 nm waveguide gaps we obtain characteristic coupling lengths $L_{\mathrm{C}} = 200 - 1000\ \mu\text{m}$. This length scale agrees well with the measured pull-in coupling lengths, L_{PI}, for *coupler 1a* and *coupler 2b* (Table II). For *coupler 3b* we initially obtain lower coupling with increasing voltage due to destructive interference, in agreement with the coupled-mode theory assuming single-mode waveguides.

If higher-order modes contribute significantly to coupling, we should see much stronger coupling than what is predicted by simulation (see Fig. 3). This stronger coupling should result in significantly shorter characteristic coupling lengths, L_{C}. However, the experimental results are in good agreement with simulation based on the fundamental mode, both in the coupling lengths required as well as the polarization-dependence. Furthermore, due to our suspended waveguide design in which we utilize tethers for support [35], higher order modes will experience increased losses compared to the first-order mode. The reason for this increased loss is the tighter confinement of the fundamental mode to the core of the waveguide, while higher order modes are less confined. Therefore, the fundamental mode dominates optical coupling from the BAR to the CROSS waveguide.

In order to obtain more efficient coupling with greater than 66% coupled power to the CROSS waveguide, we can change either 1) the coupling coefficient, κ, or 2) the physical coupling length, L_{PI}. From Table II we see that the coupling coefficient, κ, is relatively constant for different devices and actuation voltages. From κ and (5) we obtain the characteristic coupling length, L_{C}, which determines the 100% coupling length. Looking at Table II, we see that the physical coupling length is well below the characteristic coupling length, so that $L_{\mathrm{PI}} < L_{\mathrm{C}}$ for *coupler 1a* and *coupler 2b*. In order to increase coupling in our devices to 100% we therefore need to increase the pull-in length to $L_{\mathrm{PI}} = L_{\mathrm{C}}$. Alternatively, by designing narrower single-mode waveguides (width $< 2\ \mu\text{m}$) the evanescent field is increased, resulting in a larger coupling coefficient, κ, and increased coupled power.

A secondary consideration for the incomplete coupling is higher order modes. The coupling length of any higher-order modes will differ from that of the fundamental mode. Therefore, any power propagating in higher order modes may not be completely coupled to the CROSS waveguide. In general, however, optical power is concentrated in the fundamental mode. This is supported by the good agreement between our single-mode simulations and the experimental results.

Despite these considerations, we point out that the MEMS couplers in this work exhibit strong switching contrast. *Coupler 1a* shows -47 dB channel isolation at $V = 0$, with 10% (-10 dB) coupled power at pull-in. This represents a 37 dB ON/OFF contrast for the CROSS waveguide, sufficient for many switching applications.

B. Other MEMS Coupler Designs

For long-haul optical communications, single-mode fibers and optical switches are needed. Single-mode waveguides are obtained by simply reducing the cross-sectional area down to $0.5\ \mu\text{m} \times 0.5\ \mu\text{m}$ [45]. While such small cross-section may impact the mechanical robustness of the device, other materials (i.e. silicon-on-insulator) can be substituted in place of InP for passive device operation. By reducing the waveguide cross-section, the evanescent field increases so that more optical power travels just outside of the waveguide. Simulations have shown that devices with waveguide widths of $0.7\ \mu\text{m}$ enable characteristic coupling lengths of $L_{\mathrm{C}} < 100\ \mu\text{m}$ for complete coupling for both S- and P-polarizations. Therefore, very compact devices can be realized with the present approach scaled down to single-mode waveguides. By reducing the size of our moving waveguides, high speed operation and reduced switching time can also be expected.

Another modification of the present devices concerns the actuation mechanism. Using pull-in, the coupling gap cannot be continuously varied. While we have demonstrated variable optical coupling using stiction to vary the coupling length, this impacts the long-term device operation and reliability. One alternate approach prevents pull-in by using comb-drive actuators to enable continuous tuning of the waveguide separation in variable optical couplers [see Fig. 12(a)]. Experiments using 1×2 comb-drive couplers (*coupler C-D*) have shown that this approach prevents stiction in long and compliant waveguides ($L = 4000\ \mu\text{m}$). The results (see Fig. 13) successfully demonstrate variable optical coupling. Measurements, however, show smaller coupling (tens of nW power) compared to the pull-in actuated couplers (μW power). We believe the weak coupling results from the increased waveguide gap and short coupling length during actuation in the comb-drive couplers compared to the pull-in devices, in which the waveguides come into intimate contact ($\sim$100 nm pull-in gap) over a large coupler segment during actuation. Nonetheless, the results in Fig. 13 demonstrate the feasibility of optical switching and variable optical coupling using nonpull-in type actuators, which results in increased reliability.

A second approach utilizes a third electrode to actuate the BAR waveguide while keeping the CROSS waveguide fixed [see Fig. 12(b)]. If the spacing between the BAR waveguide and the actuation electrode is greater than three times the BAR

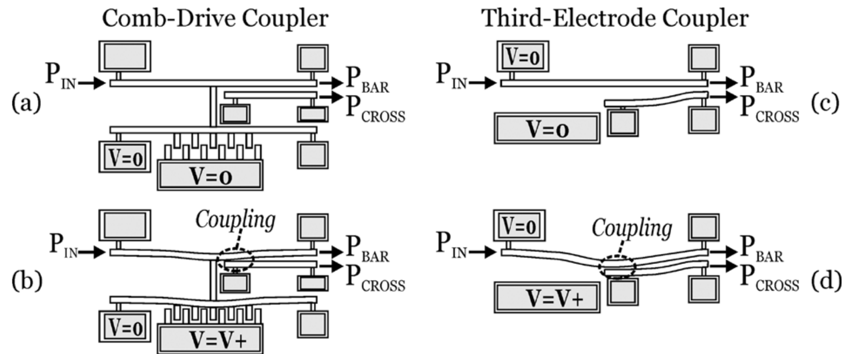

Fig. 12. Schematics for 1 × 2 couplers: (a) comb-drive coupler in rest state, (b) comb-drive coupler in actuated state, (c) third-electrode coupler in rest state, and (d) third-electrode coupler in actuated state.

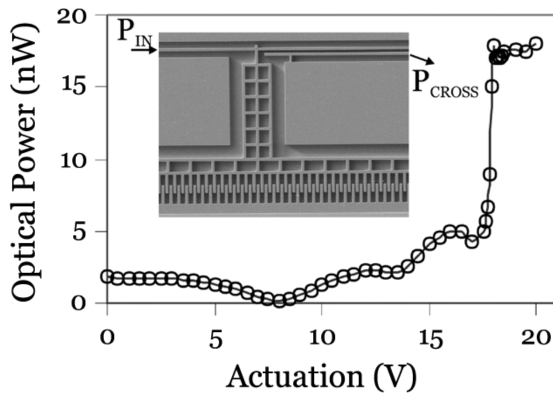

Fig. 13. Optical coupling in *coupler C-D* [1 × 2 comb-drive coupler shown in Fig. 12(a) and (b)].

to CROSS waveguide separation, then we can avoid pull-in since pull-in is known to occur after a travel range of one third the original gap [46]. This enables continuous variation of the gap and hence enables variable optical coupling.

A third approach for increasing device reliability makes use of surface coatings. Self-assembled monolayers [47] can be utilized to increase the water contact angle of InP surfaces, thereby making InP hydrophobic. This has the potential for preventing stiction in our pull-in type MEMS couplers.

C. Comparison of Device Performance

The MEMS coupler experiments show excellent performance compared with other competing designs, such as electrothermal and electro-optic coupler switches. We demonstrated low-voltage/low-power electrostatic actuation. Electrothermal couplers typically consume mW power [23], so even the μA of pull-in current in our MEMS couplers results in significantly lower power consumption. Fabrication of our devices is simple since the waveguides and actuation elements are fabricated using standard optical lithography. Although we use InP, the MEMS coupler can be implemented in low-cost silicon-based materials and does not rely on specific material properties (such as electro-optic effects [24]). The 4–20 μs switching speed is significantly faster than that of electrothermal couplers [23] as well as other MEMS optical switches [16]–[19], although it does not compare with the ns (or even sub-ns) speed obtainable with electro-optic switching. The channel isolation (at $V = 0$) of the MEMS coupler is excellent (−47 dB) due to the exponential dependence of the coupling coefficient on waveguide gap. This is a significant advantage of our MEMS approach, since small actuation distances result in large changes in coupling. Finally, while the coupling efficiency in the present devices can be improved compared to other more mature coupler approaches, single-mode waveguides with matched coupling lengths (i.e., $L_{\rm PI} = L_{\rm C}$) should result in complete coupling in our MEMS switch.

VI. Conclusion

In this paper, we have presented an all-optical InP-based MEMS waveguide switch with evanescent coupling mechanism. Our device utilizes a parallel coupling approach with electrostatic pull-in actuation. We have measured up to 66% coupling efficiency with less than 10% (0.45 dB) loss and a large channel isolation of −47 dB. We also demonstrated low-loss variable optical coupling with a 17.4 dB dynamic range. All the demonstrated devices operate at 10 V or less and are low-power. Switching times as short as 4 μs have been achieved, and reliable operation in excess of 10 million switching cycles at 10 kHz was demonstrated. We also showed evanescent coupling and switching with comb-drive actuated devices. The optical simulations are in good agreement with experimental results in terms of coupled power and polarization effects. Our switches are competitive with other MEMS approaches (mirrors, end-coupled waveguides) with regard to optical loss and required power, but with much smaller device area and the ability to continuously vary the amount of coupled power. Simulations have shown that future devices can be scaled down to single-mode waveguides with less than 1.0 μm × 1.0 μm cross-sectional areas and device lengths of 100 μm or less with no change in the basic device design. This will enable large-scale device integration for integrated optical circuits (OICs) used in network applications and photonic logic.

Acknowledgment

The authors thank L. C. Calhoun of the Laboratory for Physical Sciences (LPS) for assistance with the MBE wafer growth, L. C. Olver and the LPS staff for cleanroom access, and T. N. Ding and Dr. R. Grover for useful discussions. M. Pruessner thanks the ARCS foundation (Washington, DC chapter) for their generous fellowship support.

References

[1] C. A. Brackett, "Dense wavelength division multiplexing networks: principles and applications," *IEEE J. Sel. Areas Commun.*, vol. 8, pp. 948–964, 1990.

[2] E. Pennings, G. Khoe, M. K. Smit, and T. Staring, "Integrated-optic versus microoptic devices for fiber-optic telecommunication systems: a comparison," *IEEE J. Sel. Topics Quantum Electron.*, vol. 2, pp. 151–164, 1996.

[3] H. Fujita and H. Toshiyoshi, "Optical MEMS," *IEICE Trans. Elec.*, vol. E83, pp. 1427–1434, 2000.

[4] J. A. Walker, "The future of MEMS in telecommunications networks," *J. Micromech. Microeng.*, vol. 10, pp. R1–R7, 2000.

[5] S. Adachi, *Physical Properties of III-V Semiconductor Compounds*. New York: Wiley, 1992.

[6] S. Greek, R. Gupta, and K. Hjort, "Mechanical considerations in the design of a micromechanical tuneable InP-based WDM filter," *J. Microelectromech. Syst.*, vol. 8, pp. 328–334, 1999.

[7] S. Irmer, J. Daleiden, V. Rangelov, C. Prott, F. Römer, M. Strassner, A. Tarraf, and H. Hillmer, "Ultralow biased widely continuously tunable Fabry-Pérot filter," *IEEE Photon. Technol. Lett.*, vol. 15, pp. 434–436, 2003.

[8] J. L. Leclercq, M. Garrigues, X. Letartre, C. Seassal, and P. Viktorovitch, "InP-based MOEMS and related topics," *J. Micromech. Microeng.*, vol. 10, pp. 287–292, 2000.

[9] R. Ledantec, T. Benyattou, G. Guillot, C. Seassal, J. L. Leclercq, X. Letartre, A. Gagnaire, M. Gendry, P. Viktorovitch, R. Benferhat, D. Rondi, and R. Blondeau, "Optical characterization methods of InP-based micro-opto-electro-mechanical systems," *SPIE*, vol. 3008, pp. 258–264, 1997.

[10] R. Ledantec, T. Benyattou, G. Guillot, A. Spisser, C. Seassal, J. L. Leclercq, P. Viktorovitch, D. Rondi, and R. Blondeau, "Tunable microcavity based on InP-air Bragg mirrors," *IEEE J. Sel. Topics Quantum Electron.*, vol. 5, pp. 111–114, 1999.

[11] A. Spisser, R. Ledantec, C. Seassal, J.-L. Leclercq, T. Benyattou, D. Rondi, R. Blondeau, G. Guillot, and P. Viktorovitch, "Highly selective and widely tunable 1.55 um InP/air-gap micromachined Fabry-Perot filter for optical communications," *IEEE Photon. Technol. Lett.*, vol. 10, pp. 1259–1261, 1998.

[12] M. Strassner, J. Daleiden, N. Chitica, D. Keiper, D. Stalnacke, S. Greek, and K. Hjort, "III-V semiconductor material for tunable Fabry-Perot filters for coarse and dense WDM systems," *Sensors and Actuators A*, vol. A85, pp. 249–255, 2000.

[13] S. Greek, K. Hjort, J.-A. Schweitz, C. Seassal, J. L. Leclercq, M. Gendry, M. P. Besland, P. Viktorovitch, C. Figuet, V. Souliere, and Y. Monteil, "The strength of indium phosphide based microstructures," *SPIE*, vol. 3008, pp. 251–257, 1997.

[14] M. W. Pruessner, T. King, D. Kelly, R. Grover, L. C. Calhoun, and R. Ghodssi, "Mechanical property measurement of InP-based MEMS for optical communications," *Sens. Actuators A, Phys.*, vol. A105, pp. 190–200, 2003.

[15] E. Gini and H. Melchior, "Thermal dependence of the refractive index of InP measured with integrated optical demultiplexer," *J. Appl. Phys.*, vol. 79, pp. 4335–4337, 1996.

[16] E. Ollier, P. Labeye, and F. Revol, "Micro-opto mechanical switch integrated on silicon," *Electron. Lett.*, vol. 31, pp. 2003–2005, 1995.

[17] E. Ollier, "Optical MEMS devices based on moving waveguides," *IEEE J. Sel. Topics Quantum Electron.*, vol. 8, pp. 155–162, 2002.

[18] T. Bakke, C. P. Tigges, J. J. Lean, C. T. Sullivan, and O. B. Spahn, "Planar microoptomechanical waveguide switches," *IEEE J. Sel. Topics Quantum Electron.*, vol. 8, pp. 64–72, 2002.

[19] T. Bakke, C. P. Tigges, and C. T. Sullivan, "1 × 2 MOEMS switch based on silicon-on-insulator and polymeric waveguides," *Electronics Letters*, vol. 38, pp. 177–178, 2002.

[20] G. Keiser, *Optical Fiber Communications*, 3rd ed. Boston, MA: McGraw Hill, 2000.

[21] K. Okamoto, *Fundamentals of Optical Waveguides*. San Diego, CA: Academic, 2000.

[22] R. G. Hunsperger, *Integrated Optics: Theory and Technology*, 5th ed. Berlin, Germany: Springer, 2002.

[23] Q. Lai, W. Hunziker, and H. Melchior, "Low-power compact 2 × 2 thermooptic silica-on-silicon waveguide switch with fast response," *IEEE Photon. Technol. Lett.*, vol. 10, pp. 681–683, 1998.

[24] S. A. Samson, R. F. Tavlykaev, and R. V. Ramaswamy, "Two-section reversed switch with uniform electrodes and domain reversal," *IEEE Photon. Technol. Lett.*, vol. 9, pp. 197–199, 1997.

[25] F. Chollet, M. d. Labacherie, and H. Fujita, "Compact evanescent optical switch and attenuator with electromechanical actuation," *IEEE J. Sel. Topics Quantum Electron.*, vol. 5, pp. 52–59, 1999.

[26] G. J. Veldhuis, T. Nauta, C. Gui, J. W. Berenschot, and P. V. Lambeck, "Electrostatically actuated mechanooptical waveguide ON-OFF switch showing high extinction at a low actuation-voltage," *IEEE J. Sel. Topics Quantum Electron.*, vol. 5, pp. 60–66, 1999.

[27] M. L. Povinelli, R. E. Bryant, S. Assefa, S. G. Johnson, S. Fan, A. A. Erchak, G. S. Petrich, E. Lidorikis, J. D. Joannopoulos, L. A. Kolodziejski, and E. P. Ippen, "Design of a nanoelectromechanical high-index-contrast guided-wave optical switch for single-mode operation at 1.55 um," *IEEE Photon. Technol. Lett.*, vol. 15, pp. 1207–1209, 2003.

[28] T. Oguchi, S. Tanaka, M. Hayase, and T. Hatsuzawa, "An electro-statically driven display device using evanescent coupling between a sheet waveguide and multi-cantilevers," *Trans. Inst. Elec. Eng. Japan*, vol. 124-E, pp. 87–92, 2004.

[29] M.-C. M. Lee and M. C. Wu, "A MEMS-actuated tunable microdisk resonator," in *Proc. IEEE/LEOS Conference on Optical MEMS*, Hawaii, 2003, pp. 28–29.

[30] G. N. Nielson, D. Seneviratne, F. Lopez-Royo, P. T. Rakich, F. Giacometti, H. L. Tuller, and G. Barbasthathis, "MEMS based wavelength selective optical switching for integrated photonic circuits," *Conference on Lasers and Electro-Optics*, 2004.

[31] B. Broberg and S. Lindgren, "Refractive index of In(1-x) Ga(x)As(y)P(1-y) layers and InP in the transparent wavelength region," *J. Appl. Phys.*, vol. 55, pp. 3376–3381, 1984.

[32] R. Grover, T. A. Ibrahim, S. Kanakaraju, L. Lucas, L. C. Calhoun, and P.-T. Ho, "A tunable GaInAsP-InP optical microring notch filter," *IEEE Photon. Technol. Lett.*, vol. 16, pp. 467–469, 2004.

[33] S. S. Saini, F. G. Johnson, D. R. Stone, W. Zhou, H. Shen, and M. Dagenais, "A 2 × 2 crosspoint switch fabricated on the passive active resonant coupler (PARC) platform," *IEEE Photon. Technol. Lett.*, vol. 13, pp. 203–205, 2001.

[34] C. L. Chang, S. Wagner, and A. A. Ballmann, "Optical absoprtion tail in InP:Mn from surface photovoltage measurements," *Appl. Phys. Lett.*, vol. 43, pp. 1113–1115, 1983.

[35] D. Kelly, M. W. Pruessner, K. Amarnath, M. Datta, S. Kanakaraju, L. C. Calhoun, and R. Ghodssi, "Monolithic suspended optical waveguides for InP MEMS," *IEEE Photon. Technol. Lett.*, vol. 16, pp. 1298–1300, 2004.

[36] *Optical Waveguide Mode Solver (OWMS): Version 1.21 ed.*, Apollo Photonics, Waterloo, Canada, 1997–2001.

[37] P. M. Osterberg and S. D. Senturia, "M-Test: a test chip for MEMS material property measurement using electrostatically actuated test structures," *J. Microelectromech. Syst.*, vol. 6, pp. 107–118, 1997.

[38] M. W. Pruessner, K. Amarnath, M. Datta, D. Kelly, K. Subramaniam, P.-T. Ho, and R. Ghodssi, "Optical and mechanical characterization of an evanescent coupler optical switch," in *Proc. Solid-State Sensor, Actuator, and Microsystems Workshop*, Hilton Head Island, SC, 2004, pp. 238–241.

[39] R. Maboudian and R. T. Howe, "Critical review: adhesion in surface micromechanical structures," *J. Vacuum Sci. Technol.*, vol. B15, pp. 1–20, 1997.

[40] R. J. Deri and E. Kapon, "Low-loss III-V semiconductor optical waveguides," *IEEE J. Quantum Electron.*, vol. 27, pp. 626–640, 1991.

[41] I. Moerman, P. P. Van Daele, and P. M. Demeester, "A review on fabrication technologies for the monolithic integration of tapers with III-V semiconductor devices," *IEEE J. Sel. Topics Quantum Electron.*, vol. 3, pp. 1308–1320, 1997.

[42] E. M. Garmire and K. Honda, "Depolarization in channel glass waveguides," *J. Lightw. Technol.*, vol. LT-4, pp. 220–227, 1986.

[43] B. E. Little and T. Murphy, "Design rules for maximally flat wavelength-insensitive optical power dividers using Mach-Zehnder structures," *IEEE Photon. Technol. Lett.*, vol. 9, pp. 1607–1609, 1997.

[44] T. E. Murphy, B. E. Little, and H. I. Smith, "Wavelength- and polarization-insensitive integrated directional couplers," *Integrated Photonics Research Conference*, 1999.

[45] R. Grover, T. A. Ibrahim, T. N. Ding, Y. Leng, L.-C. Kuo, S. Kanakaraju, K. Amarnath, L. C. Calhoun, and P.-T. Ho, "Laterally coupled InP-based single-mode microracetrack notch filter," *IEEE Photon. Technol. Lett.*, vol. 15, pp. 1082–1084, 2003.

[46] S. D. Senturia, *Microsystem Design*. Boston, MA: Kluwer Academic, 2000.

[47] H. Lim, C. Carraro, R. Maboudian, M. W. Pruessner, and R. Ghodssi, "Chemical and thermal stability of alkanethiol and sulfur passivated InP(100)," *Langmuir*, vol. 20, pp. 743–747, 2004.

Marcel W. Pruessner (S'00) received the B.S., M.S., and Ph.D. degrees in electrical engineering from the University of Maryland, College Park, in 1998, 2002, and 2005, respectively.

In 1999, he worked at the U.S. Patent and Trademark office as a Patent Examiner in the general area of circuits and devices. From 1999 to 2000, he was employed as a Faculty Research Assistant at the Institute for Plasma Research (now the Institute for Research in Electronics and Applied Physics) at the University of Maryland. His research focused on electron beam position sensing and control for an accelerator project. Since 2000, he has been a graduate research assistant in the MEMS Sensors and Actuators Lab (MSAL) at the University of Maryland, where his work focuses on indium phosphide (InP) optical waveguide MEMS for communications and sensing applications.

Mr. Pruessner is a Member of Phi Beta Kappa, and he is the recipient of a 2003–2004 ARCS fellowship (Metropolitan Washington, DC Chapter).

Kuldeep Amarnath received the B.Tech. degree in engineering physics from the Indian Institute of Technology, Bombay, India, in 1998. While there, he also worked on projects in Observational Cosmology at the Inter-University Center for Astronomy and Astrophysics, Pune, and the Tata Institute of Fundamental Research, Bombay. He is currently a Doctoral candidate in the Department of Electrical and Computer Engineering at the University of Maryland, College Park.

In addition to optical MEMS, his research interests include the development of active microring resonators for use in photonic logic circuits. He is a recipient of the Army Research Labs graduate research fellowship.

Madhumita Datta (S'98–M'02) received the M.S. and Ph.D. degrees in electrical and computer engineering, both from the University of Maryland, College Park, in 1999 and 2002, respectively. Prior to that, she received the B.S. degree in electrical engineering from Jadavpur University, Calcutta, India, in 1995. Her doctoral research was on hybrid integration and packaging of optoelectronic and fiber-optic modules for telecom and datacom applications.

As part of her postdoctoral research at the MEMS Sensors and Actuators Laboratory at the University of Maryland, College Park, she works on MEMS-tunable wavelength-selective integrated photonic devices for reconfigurable wavelength division multiplexing (WDM) networks and BioMEMS applications. She has published a number of peer-reviewed articles on optoelectronic packaging and optical MEMS in various international journals and conference proceedings, and holds one U.S. patent.

Daniel P. Kelly was born in Silver Spring, MD, in 1980. He received the B.S. degree in electrical engineering from the University of Maryland, College Park, in 2002 and is currently pursuing the M.S. degree in electrical engineering at the University of Maryland, College Park, with research focused on InP MEMS.

He is currently with the NASA Goddard Space Flight Center and QSS Group, Inc., working on Microshutter Array development for the James Webb Space Telescope. His research interests include optical MEMS (MOEMS) and integration of optoelectronic materials such as indium phosphide in MEMS devices.

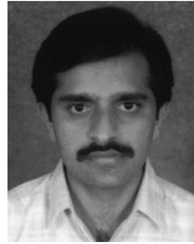

S. Kanakaraju received the Ph.D degree from Indian Institute of Science, Bangalore, India, in 1998.

He worked as a research associate at the University of Virginia (1998–2001) where he was involved in the development of *in situ* sensors for thin-film growth monitoring. He is with the Laboratory for Physical Sciences since 2001. His research interests cover epitaxial growth and characterization of semiconductor heterostructures for optoelectronic and photonic devices.

Ping-Tong Ho biography and photograph not available at the time of publication.

Reza Ghodssi (S'92–M'97) received the B.S., M.S., and Ph.D. degrees in electrical engineering from the University of Wisconsin at Madison, in 1990, 1992, and 1996, respectively.

He was a Postdoctoral Associate and a Research Scientist in the Microsystems Technology Laboratories and the Gas Turbine Laboratory at the Massachusetts Institute of Technology (MIT), Cambridge, from 1997 until 1999. During his tenure at MIT, he developed the building block MEMS fabrication technologies for a microturbine generator device and also served as an Assistant Director on that project. He is Director of the MEMS Sensors and Actuators Laboratory (MSAL) and an Associate Professor in the Department of Electrical and Computer Engineering and the Institute for Systems Research (ISR) at the University of Maryland (UMD). He is also a core faculty member in the Bioengineering Graduate Program and Small Smart Systems Center (SSSC) at UMD. His research interests are in design and development of microfabrication technologies and their applications to microsensors, microactuators, and integrative microsystems.

Dr. Ghodssi was awarded the 2001 UMD George Corcoran Award, 2002 National Science Foundation CAREER Award, and the 2003 UMD Outstanding Systems Engineering Faculty Award. He has served as a Program Co-Chairman for the 2001 International Semiconductor Device Research Symposium (ISDRS) and as a Chairman of the MEMS and NEMS Technical Group at the American Vacuum Society (AVS), from 2002 to 2004. He is a Co-Founder of the MEMS Alliance Group in the greater Washington area and a member of the AVS, MRS, AAAS, and ASEE societies.